CORA Cork Open Research Archive
Cartlann Taighde Oscailte Chorcaí

Title	A bandwidth enhanced 915 MHz antenna for IoT wrist-watch applications
Authors	Kumar, Sanjeev;Buckley, John;Barton, John;Newberry, Robert;Dunlop, Gary;Rodencal, Matthew;Webster, Carlo;O'Flynn, Brendan
Publication date	2019
Original Citation	Kumar, S., Buckley, J. L., Barton, J., Newberry, R., Dunlop, G., Rodencal, M., Webster, C. and O'Flynn, B. (2019) 'A bandwidth enhanced 915 MHz antenna for IoT wrist-watch applications', 13th European Conference on Antennas and Propagation (EuCAP 2019), Krakow, Poland, 31 March-5 April, pp. 1-5.
Type of publication	Conference item
Link to publisher's version	https://www.eucap.org/, https://www.eucap.org/files/eucap-2019-final-programme-update
Rights	© 2019, European Association on Antennas and Propagation (EurAAP). All rights reserved.
Download date	2026-09-09 15:55:12
Item downloaded from	https://hdl.handle.net/10468/7861

UCC
University College Cork, Ireland
Coláiste na hOllscoile Corcaigh

A Bandwidth Enhanced 915 MHz Antenna for IoT Wrist-Watch Applications

Sanjeev Kumar[1], John L. Buckley[1], John Barton[1], Robert Newberry[2], Gary Dunlop[2],

Matthew Rodencal [2], Carlo Webster[1], Brendan O' Flynn[1]

[1] Tyndall National Institute, University College Cork, Cork, Ireland, Sanjeev.kumar@tyndall.ie

[2] Sanmina Corporation, 13000 S. Memorial Parkway, Huntsville, AL 35803, USA.

***Abstract*— This paper presents a 915 MHz planar inverted-F antenna (PIFA) topology for a wrist-worn wireless sensor application. When compared with a conventional PIFA implementation, an impedance bandwidth enhancement of more than 100% is achieved. The bandwidth enhancement is realized with inclusion of a parasitic element that excites an additional mode close to the resonant frequency. A parametric analysis of the key parameters is performed in order to optimize the antenna for 915 MHz operation. The measured results for the on-body prototype antenna show a -10 dB bandwidth of 26.4 MHz and a Peak Realized Gain of -0.57 dBi at 915 MHz. The simulated peak radiation efficiency of 46.8% is achieved. In addition, the design exhibits a low specific absorption rate (SAR) value of 0.004 W/kg.**

***Index Terms*— Antenna, bandwidth enhancement, wristwatch, Sub-GHz, PIFA, wearable.**

I. INTRODUCTION

In recent years, wrist-watches equipped with physiological sensors are emerging in a growing number of Internet of Things (IoT) applications. Such devices with wireless capability can play a significant role in healthcare applications such as bio-physiological measurements of heart rate, temperature and arterial oxygen saturation (SpO2) [1, 2]. Presently, 2.45 GHz band antennas are in widespread use for wearable wrist-worn IoT applications [3, 4]. In [2], the 915 MHz band for future IoT wearable applications is investigated and is shown that communications at 915 MHz can lead to reduced free space path loss, improved link budget and reduced interaction with the body in comparison to the 2.45 GHz band. Thus, Sub-GHz communications has the potential to become an alternative to the conventional 2.45 GHz band. The 915 MHz wearable planar inverted-F antenna (PIFA) reported in [2] has an on-body measured peak realized gain of -6.1 dBi. A 55 MHz of -10 dB impedance bandwidth was achieved using a π-type matching network. In [5], three types of dipole and monopole based smart-watch antennas using a metallic strap that operates in the 700 MHz to 2.7 GHz cellular band are presented. These antennas offer a wide bandwidth, especially the dipole antenna exhibits a good impedance bandwidth of approximately 160 MHz at Sub-GHz frequencies. However, these antennas in on-body scenario results in low radiation efficiency of less than 10% at 900 MHz. A dual band loop antenna using a metallic wristwatch frame is presented in [6] and has an impedance bandwidth of 80 MHz, but this antenna also has low efficiency of less than 15% at Sub-GHz frequencies. A wristband helical RFID antenna is reported in [7] and meets the bandwidth requirement of 3 MHz for UHF band but this antenna has a low on-body realized gain of -13 dBi.

This work aims to maximize both the bandwidth and gain of the antenna. A bandwidth enhancement technique using a parasitic element similar to [8, 9] is implemented. The proposed antenna topology includes a coplanar parasitic element that excites an additional mode close to the resonant frequency denoted f_0 = 915 MHz and improves the antenna impedance bandwidth by more than 100%. The performance characteristics of the antenna were first simulated using Ansys HFSS full-wave EM analysis [10] and then the prototype was fabricated and measured. The simulated and measured results are shown to be in good agreement.

II. ANTENNA DESIGN

The configuration of the proposed wristwatch antenna is shown in Fig. 1. The antenna is a variant of a PIFA topology and is integrated within a wristwatch enclosure. The enclosure material uses acrylonitrile butadiene styrene (ABS) plastic with a dielectric constant ε_r = 2.8 and a loss tangent 0.004 at 1 GHz [11]. The overall dimension of the enclosure is 50×35×15 mm^3. The total size of the antenna element and the ground plane is 43.5×28.5 mm^3 and is excited at point '*P*' using a 50-Ω coaxial feed. The main radiator (driven element) is made of 0.35 mm copper plate and extends between point *A* and *B*. The total length of the driven element is 208.5 mm that corresponds to a free-space electrical length of $0.635\lambda_0$ at 915 MHz. A ground connected parasitic element is used for the purpose of bandwidth enhancement. The parasitic element extends between points *A* and *C* with an electrical length of approximately $\lambda_0/4$ at 915 MHz. As explained in [12], an inductive shorting plate is used to match the impedance of the antenna to 50-Ω. The wristwatch strap used in this work is made of silicone rubber with a dielectric constant ε_r = 2.95 and a loss tangent of 0.001 at 1 GHz [13]. As shown in Fig.1(b) a cylindrical homogeneous phantom arm of 200 mm height and 63 mm diameter with dielectric constant ε_r = 35.76, electrical conductivity σ = 0.58 S/m and mass density

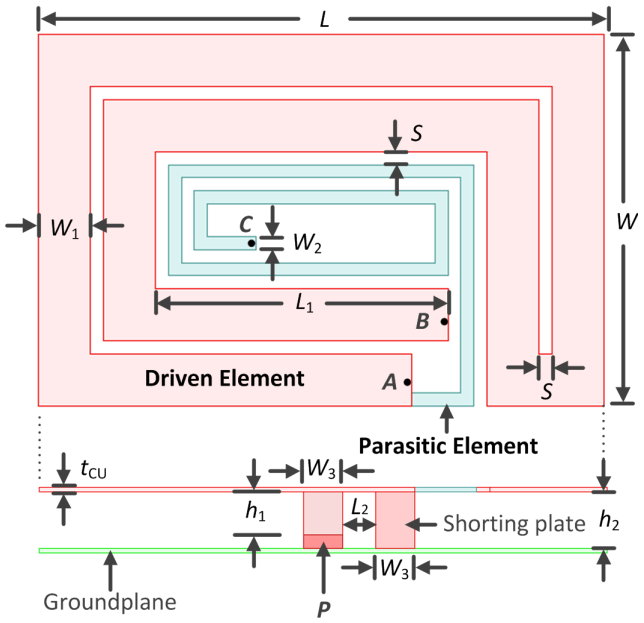

(a)

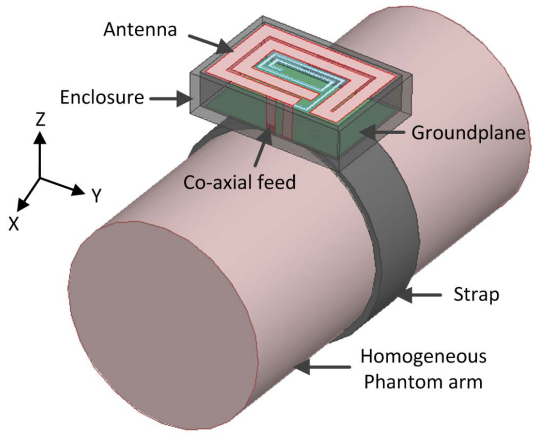

(b)

Fig. 1. (a) Configuration of the proposed 915 MHz antenna (b) Antenna with enclosure placed on the phantom arm.

ρ = 1764 kg/m^3 at 915 MHz was used to mimic the human wrist [14].

III. Antenna Simulations

In this section, the simulated results of the conventional quarter-wavelength PIFA [8] are first presented. It has been discussed in [15] that, in general, most of the multiband antennas are resonant at fundamental mode and its harmonics or close to harmonic of the fundamental resonant mode. The simulated reflection coefficient in Fig. 2 shows the first and second harmonics of the antenna over the 0.2-1GHz frequency range. It can be seen that the fundamental resonance (f_{01}) of the antenna is 485 MHz. Corresponding to the fundamental mode, the antenna exhibits a -10 dB impedance bandwidth of 6.1 MHz, which does not meet the required specification of ≥ 26 MHz at 915 MHz applications

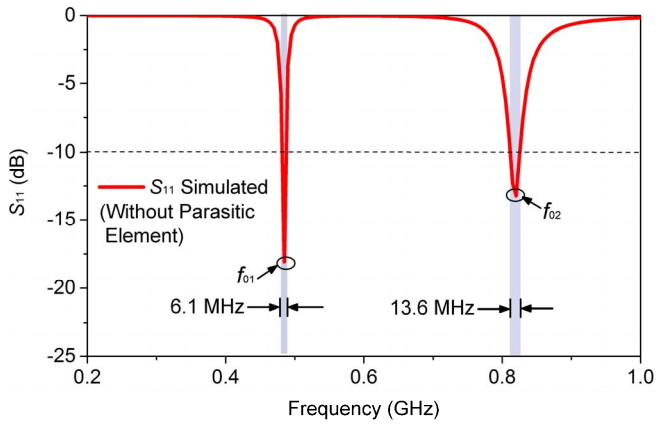

Fig. 2. Simulated S_{11}, showing first and second harmonics of a conventional PIFA without parasitic element.

[16]. However, the second harmonic f_{02} is resonant at 820 MHz with a -10 dB impedance bandwidth of 13.9 MHz. Thus, in this study the second harmonic mode is investigated in detail to try to meet the 26 MHz impedance bandwidth requirements [16].

A. Bandwidth Enhancement

For a given frequency and antenna physical size, there is a theoretical limit on the maximum achievable bandwidth [17]. Thus, due to space limitations, it is challenging to design a compact wristwatch antenna satisfying the minimum -10 dB impedance bandwidth requirement of 26 MHz at the 915 MHz band. In the proposed antenna design, a coplanar parasitic element is incorporated that excites an additional resonant mode close to the resonant frequency of the driven element. In Fig. 3, -10 dB simulated impedance bandwidth of the antenna *with* and *without* the parasitic element is presented. With no parasitic element the antenna is resonant at f_{02} = 820 MHz with a -10 dB impedance bandwidth of 13.6 MHz. When the parasitic element is included, the resonant frequency shifts to f_0 = 915 MHz with a -10 dB impedance bandwidth of 32.7 MHz or an improvement of greater than 100%.

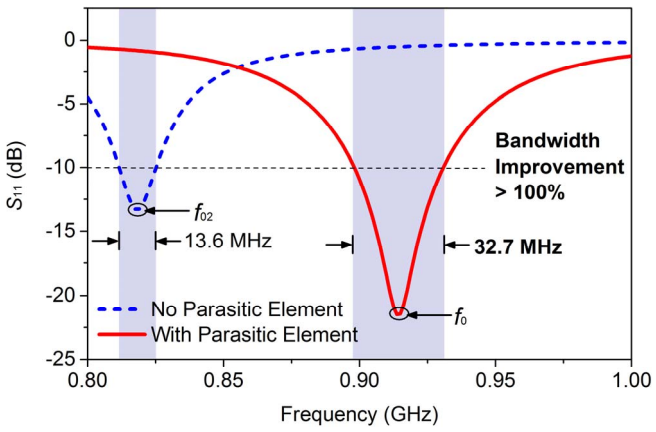

Fig. 3. Bandwidth enhancement using parasitic element.

B. Parametric Analysis

A parametric analysis was conducted in order to optimize the antenna geometry for 915 MHz operation. For this purpose, the effect of several key parameters on the resonant behavior of the antenna was investigated. The influence of the parameter L_1, which determines the total length of the driven element was studied. Parameter L_1 was varied from 5 mm to 20 mm, while keeping all the parameters fixed as listed in Table I, and the corresponding S_{11} response is plotted in Fig. 4 (a). The resonant frequency continuously decreases with increasing L_1 and it has little effect on the impedance matching and -10 dB impedance bandwidth of the antenna.

Secondly, the influence of the driven element width, W_1 on the resonant behavior was investigated. It is important to note that varying W_1 also changes the separation (S) between the consecutive arms of the driven element, because $(2 \times W_1) + S =$ constant. The response of the antenna with varying W_1 between 3 mm to 4.5 mm, while keeping other parameters as in Table I, is summarized in Fig. 4 (b). The resonant frequency of the antenna increases continuously as W_1 increases from 3 mm to 4.5 mm. The antenna is resonant at 915 MHz for $W_1 = 4$ mm. The -10 dB impedance bandwidth improves with increasing the value of the parameter W_1. The parameter L_2 is defined as the distance of the feedline location (L_2) from the shorting plate. The parameter L_2 was varied in the range of 2.5 mm to 5.5 mm while keeping the other parameters constant as listed in Table I. The resulting S_{11} response is shown in Fig.4 (c). The resonant frequency increases continuously with increasing L_2 and the antenna is resonant at 915 MHz for $L_2 = 2.5$ mm. Also, the impedance bandwidth decreases with increasing the value of L_2. In comparison to L_1 and W_1, the parameter L_2 has more impact on the impedance matching behavior of the antenna. It is concluded from the parametric analysis that the parameters L_1, W_1 and L_2 enables sufficient degree of freedom to tune the resonant frequency and control -10 dB bandwidth and impedance matching of the antenna. The final dimensions of the proposed antenna are listed in Table I.

Table I
Final Parameters of the Proposed Antenna

Parameter	Value (mm)	Parameter	Value (mm)
L	43.50	W_3	3.00
L_1	22.50	t_{CU}	0.35
L_2	2.50	S	1.00
W	28.50	h_1	8.30
W_1	4.00	h_2	10.30
W_2	1.00		

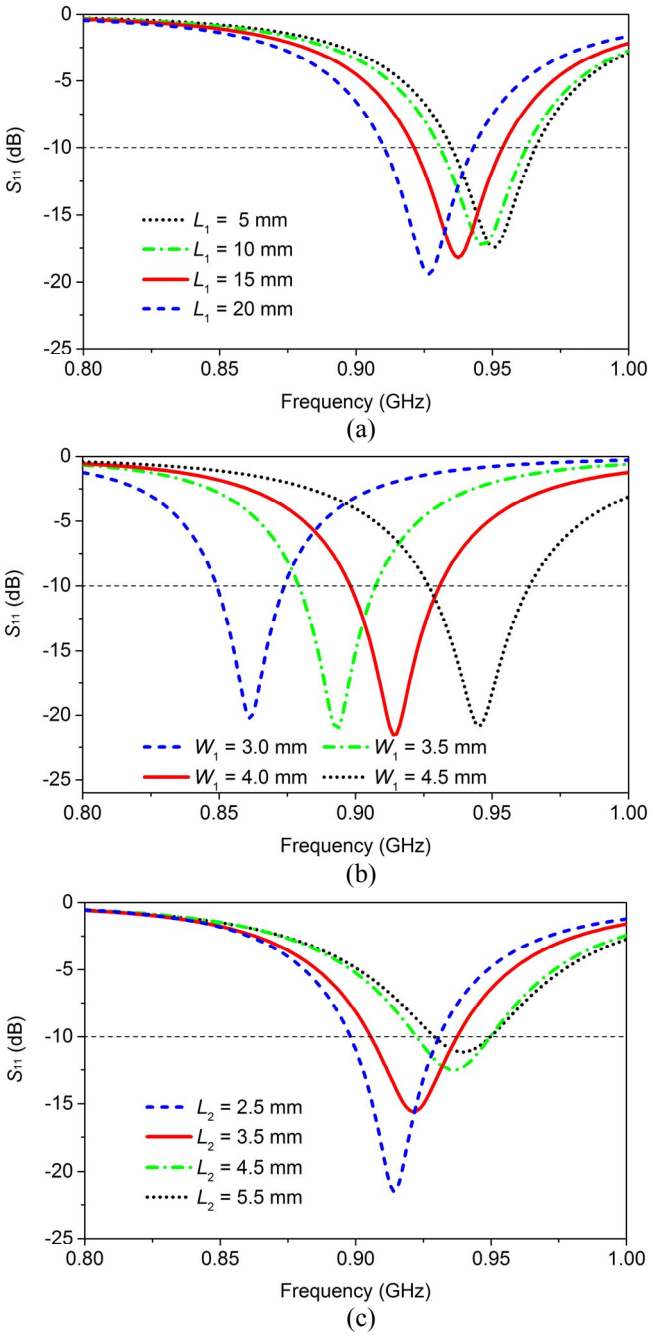

Fig. 4. Simulated S_{11} for (a) varying L_1, (b) varying W_1 and (c) varying L_2.

C. Surface Current and SAR Distribution

Fig. 5 shows the surface current distribution on the driven and parasitic elements at 915 MHz. Large currents are observed, indicating that both elements are resonant at $f_0 = 915$ MHz.

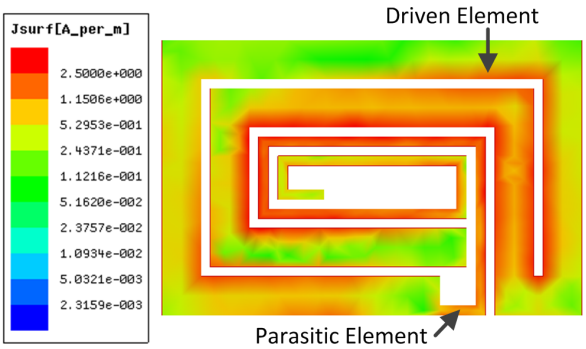

Fig. 5. Surface current distribution of the antenna at 915 MHz.

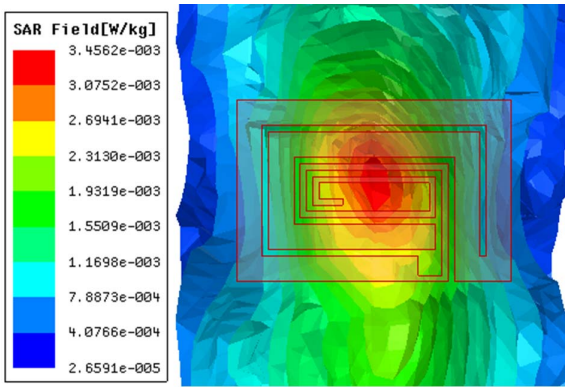

Fig. 6. SAR distribution on phantom arm at 915 MHz.

In Fig. 6 the simulated specific absorption rate (SAR) [4] on the phantom arm is presented. The obtained peak 1g SAR for an input power of 1mW was 0.004 W/kg; this is less than 2.5% of the legal SAR limit of 1.6 W/kg defined in [5]. In addition, the simulated peak radiation efficiency and the peak realized gain at 915 MHz were 46.8% and -0.77 dBi, respectively.

IV. Antenna Measurements

In this section, the measured impedance and radiation characteristics of the antenna are presented. As shown in Fig. 7 (a), the copper radiator was fabricated using a CAD controlled Bridgeport GX-480 milling machine [18]. The measurements were taken after placing the antenna under test (AUT) on a homogeneous phantom arm as shown in Fig. 7 (b). The S_{11} response was measured using Rohde & Schwarz ZVRE vector network analyzer (VNA) [19]. The simulated and measured S_{11} results are shown in Fig. 8. The difference between simulated and measured response is attributed to the imperfect measurement environment and fabrication tolerance. As shown in Fig. 7 (c) the radiation pattern measurements were performed in an AMS-8050 antenna measurement system [20]. The measured and simulated radiation characteristics are shown in Fig. 9. For the co-polarized case, the *xy*-plane exhibits an omnidirectional radiation pattern and in *yz*-plane, the

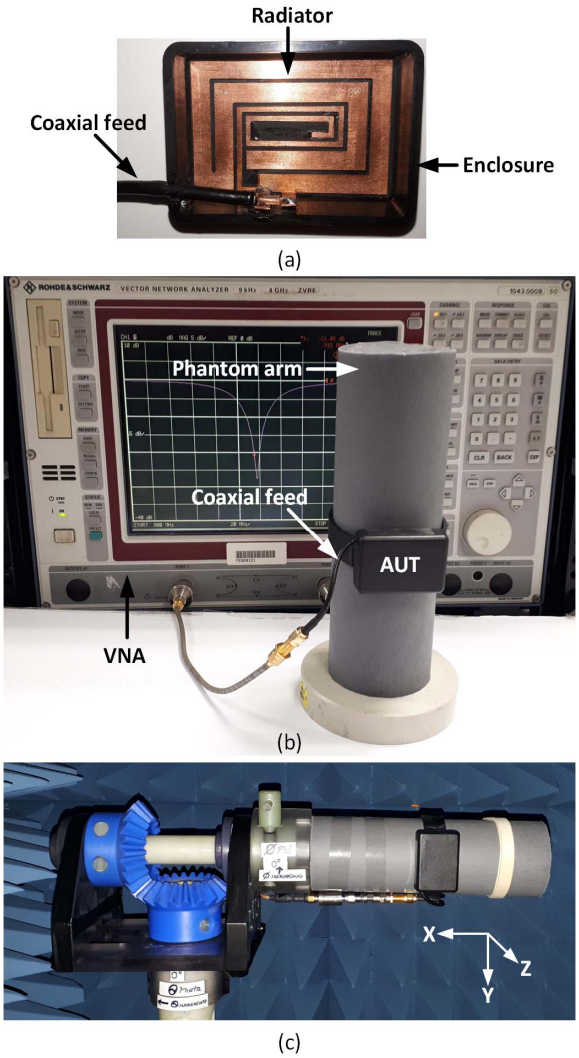

Fig.7. (a) Antenna prototype, (b) VNA measurement setup, (c) AUT measurement setup in AMS-8050 anechoic chamber [20].

antenna has a dipole-like radiation characteristic. In *xz*-plane, the obtained radiation characteristic has a pseudo omni-directional pattern.

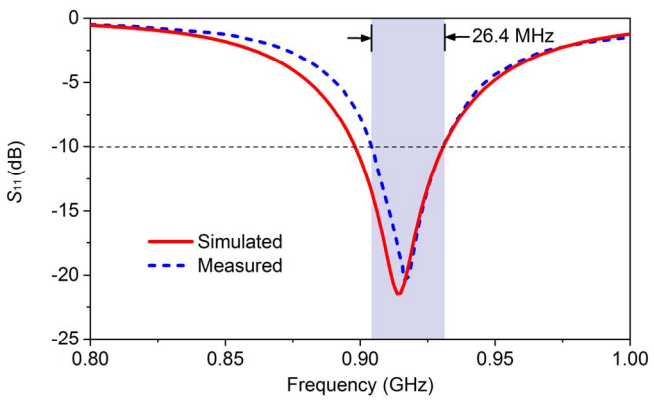

Fig. 8. Simulated versus measured S_{11} results.

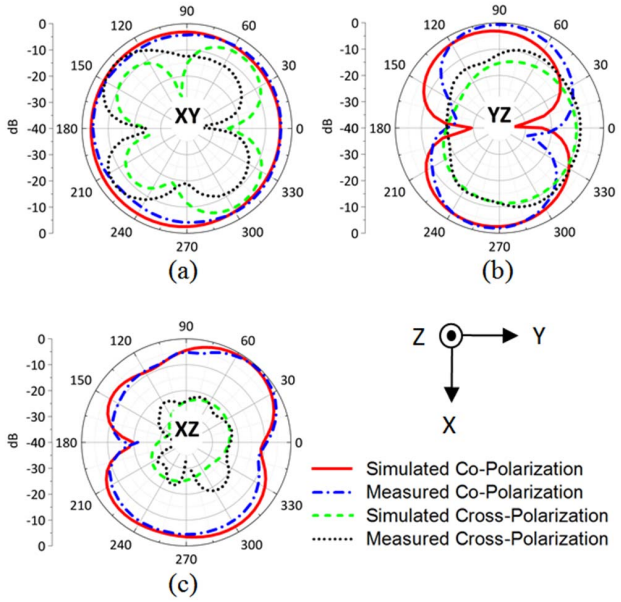

Fig. 9. Simulated and measured radiation characteristics of the antenna at 915 MHz (a) *xy*- plane (b) *yz*- plane and (c) *xz*- plane.

Overall, a good agreement between simulated and measured radiation characteristics with a measured peak realized gain of -0.57 dBi at 915 MHz, compared to -0.77 dBi for the simulated case is achieved.

V. Conclusion

A meandered PIFA topology for wristwatch applications at 915 MHz has been presented. In comparison to a conventional PIFA, over 100% bandwidth enhancement was achieved by employing a coplanar parasitic element while maximizing the gain of the antenna. A parametric analysis was conducted in order to analyze the influence of several key parameters and optimize the antenna geometry for 915 MHz operation. A good agreement between simulated and measured results is demonstrated. At 915 MHz the measured results have a -10 dB impedance bandwidth of 26.4 MHz and a peak realized gain of -0.57 dBi. A simulated peak radiation efficiency of 46.8% has been achieved. Moreover, for an input power of 1mW, a peak SAR of 0.004 W/kg has been demonstrated.

VI. Acknowledgements

We would like to acknowledge the support of Enterprise Ireland and the IDA for funding Innovation Partnership Project No IP20170559. We also acknowledge support from Science Foundation Ireland under grant 13/RC/2077 (CONNECT) as well as the support of Andrew Wallace and team from National Instruments for their continued support with the AWR toolset. This project is co-funded by the European Regional Development Fund (ERDF) under Ireland's European Structural and Investment Funds Programmes 2014-2020.

References

[1] E. Jovanov, "Preliminary analysis of the use of smartwatches for longitudinal health monitoring," *Annual International Conference of the IEEE Engineering in Medicine and Biology Society,* vol. 37, pp. 865-868, 25-29 Aug. 2015.

[2] A. D. Serio, J. Buckley, J. Barton, R. Newberry, M. Rodencal, G. Dunlop and B. O'Flynn, "Potential of Sub-GHz Wireless for Future IoT Wearables and Design of Compact 915 MHz Antenna," *Sensors,* vol. 18, no. 1, 2018.

[3] S. Su and Y. Hsieh, "Integrated Metal-Frame Antenna for Smartwatch Wearable Device," *IEEE Transactions on Antennas and Propagation,* vol. 63, no. 7, pp. 3301-3305, 2015.

[4] D. Wu and S. W. Cheung, "A Cavity-Backed Annular Slot Antenna With High Efficiency for Smartwatches With Metallic Housing," *IEEE Transactions on Antennas and Propagation,* vol. 65, no. 7, pp. 3756-3761, 2017.

[5] K. Zhao, Z. Ying, and S. He, "Antenna designs of smart watch for cellular communications by using metal belt," *European Conference on Antennas and Propagation,* pp. 1-5, 2015.

[6] C. Hong and S. Yeh, "Cellular antenna design with metallic housing for wearable device," *Asia-Pacific Conference on Antennas and Propagation,* pp. 419-420, 2016.

[7] S. Lopez-Soriano and J. Parron, "Design of a Small-Size, Low-Profile, and Low-Cost Normal-Mode Helical Antenna for UHF RFID Wristbands," *IEEE Antennas and Wireless Propagation Letters,* vol. 16, pp. 2074-2077, 2017.

[8] H. T. Chattha, Y. Huang, M. K. Ishfaq, and S. J. Boyes, "Bandwidth enhancement techniques for planar inverted-F antenna," *IET Microwaves Antennas & Propagation,* vol. 5, no. 15, pp. 1872-1879, 2011.

[9] A. çelebi, T. Wong, and M. Kenkel, "A TBH antenna with parasitic element for bandwidth enhancement," *IEEE International Symposium on Antennas and Propagation,* pp. 1-2, 2012.

[10] ANSYS HFSS, Available online: *http://www.ansys.com/products/electronics/ansys-hfss, Accessed in July 2018.*

[11] A. Helminen and T. Kiikka, *Premix: Optimizing RF Properties of Injection Molded Plastic Parts, Available online: https://www.premixgroup.com/, Accessed in July 2018.,* 2014.

[12] J. Buckley, D. Gaetano, K. G. McCarthy, L. Loizou, B. O' Flynn and C. O' mathuna, "Compact 433 MHz antenna for wireless smart system applications." *Electronics Letter.* Vol. 50, pp. 572-574, 2014.

[13] J. F. Dexter and P. C. Servais, "Silicone rubber as cable insulation," *Wire and Cable Symposium, U. S Army Signal Corps,* 1967.

[14] Indexsar IXB-060 phantom column, Available online: *https://indexsar.com/product/phantom-columns-ixb-063-and-ixb-103/, Accessed in July 2018.*

[15] J. L. Buckley, K. G. McCarthy, L. Loizou, B. O. Flynn, and C. O. Mathuna, "A Dual-ISM-Band Antenna of Small Size Using a Spiral Structure With Parasitic Element," *IEEE Antennas and Wireless Propagation Letters,* vol. 15, pp. 630-633, 2016.

[16] K. Eroglu, "The worldwide approval status for 900 MHz and 2.4 GHz spread spectrum radio products," *International Symposium on Electromagnetic Compatibility,* vol. 2, pp. 1131-1135 1998.

[17] R. F. Harrington, "Effect of Antenna Size on Gain, Bandwidth, and Efficiency," *Journal of Research of the National Bureau of Standards- D. Radio Propagation,* vol. 64D, 1960.

[18] Bridgeport GX 480 System. Available online: *http://bpt.com/ProductCatalog/Product/ProductId/173 . Accessed in September 2018.*

[19] Rohde & Schwarz ZVRE vector network analyzer . Available online: *https://www.rohde-schwarz.com . Accessed in October 2018.*

[20] ETS-LINDGREN: AMS-8050 Antenna Measurement System. Available online: *http://www.ets-lindgren.com/ . Accessed in October 2018.*